

This is a repository copy of *Highly stable AgNPs prepared via a novel green approach for catalytic and photocatalytic removal of biological and non-biological pollutants*.

White Rose Research Online URL for this paper:

<https://eprints.whiterose.ac.uk/164628/>

Version: Published Version

Article:

Rani, Pooja, Kumar, Vanish, Singh, Prit Pal et al. (5 more authors) (2020) Highly stable AgNPs prepared via a novel green approach for catalytic and photocatalytic removal of biological and non-biological pollutants. *Environment International*. 105924. ISSN 0160-4120

<https://doi.org/10.1016/j.envint.2020.105924>

Reuse

This article is distributed under the terms of the Creative Commons Attribution (CC BY) licence. This licence allows you to distribute, remix, tweak, and build upon the work, even commercially, as long as you credit the authors for the original work. More information and the full terms of the licence here:

<https://creativecommons.org/licenses/>

Takedown

If you consider content in White Rose Research Online to be in breach of UK law, please notify us by emailing eprints@whiterose.ac.uk including the URL of the record and the reason for the withdrawal request.



Highly stable AgNPs prepared via a novel green approach for catalytic and photocatalytic removal of biological and non-biological pollutants

Pooja Rani^{a,1}, Vanish Kumar^{b,1}, Prit Pal Singh^c, Avtar Singh Matharu^d, Wei Zhang^e,
Ki-Hyun Kim^{f,*}, Jagpreet Singh^{a,*}, Mohit Rawat^{a,*}

^a Department of Nanotechnology, Sri Guru Granth Sahib World University, Fatehgarh Sahib 140406, Punjab, India

^b National Agri-Food Biotechnology Institute (NABI), S.A.S. Nagar, Punjab 140306, India

^c Department of Chemistry, Sri Guru Granth Sahib World University, Fatehgarh Sahib 140406, Punjab, India

^d Green Chemistry Centre of Excellence, Department of Chemistry, University of York, York YO10 5DD, UK

^e School of Ecology and Environmental Science, Zhengzhou University, 100 Kexue Avenue, Zhengzhou, Henan 450001, PR China

^f Department of Civil & Environmental Engineering, Hanyang University, Seoul 04763, South Korea

ARTICLE INFO

Handling Editor: Adrian Covaci

Keywords:

Phaseolus Vulgaris
Silver nanoparticles
Green synthesis
4-nitrophenol
Catalytic activity
Photocatalytic degradation

ABSTRACT

Increases in biological and non-biological pollutants pose a significant threat to environmental systems. In an effort to develop an effective means to treat such pollutants, the use of *Phaseolus vulgaris* (kidney beans) as reducing and capping agents is proposed for the green synthesis of highly stable silver nanoparticles (AgNPs) with a face-centered cubic (fcc) crystalline structure (size range: 10–20 nm). The potent role of the resulting AgNPs was found as triple platforms (photocatalyst, catalyst, and antimicrobial disinfectant). AgNPs were able to photocatalytically degrade approximately 97% of reactive red-141 (RR-141) dye within 150 min of exposure (quantum efficiency of 3.68×10^{-6} molecule.photon⁻¹ and a removal reaction kinetic rate of 1.13×10^{-2} mmol g⁻¹ h⁻¹). The role of specific reactive oxygen species (ROS) in the photocatalytic process and complete mineralization of dye was also explored through scavenger and chemical oxygen demand (COD) experiments, respectively. As an catalyst, AgNPs were also capable of reducing 4-nitrophenol to 4-aminophenol within 15 min. Overall, AgNPs showed excellent stability as catalyst and photocatalyst even after five test cycles. As an antimicrobial agent, the AgNPs are effective against both gram-positive (*Bacillus subtilis*) and -negative bacteria (*Escherichia coli*), with the zones of clearance as 15 and 18 mm, respectively. Thus, the results of this study validate the triple role of AgNPs derived via green synthesis as a photocatalyst, catalyst, and antimicrobial agent for effective environmental remediation.

1. Introduction

The continuous growth of global population coupled with industrialization and urbanization has brought rising demand for chemicals, materials, and energy. The release of highly undesirable wastes from numerous man-made sources into environment was inevitably accompanied to lower the quality of environmental systems, of particular aquatic reservoirs (Ali et al., 2019). For example, azo dyes (e.g., Reactive Red 141 [RR-141]: Table 1), which contain two azo groups and one sulfonic acid group, are identified as a major industrial effluent contaminating freshwater bodies. The fixation rate of reactive dyes in the dying process is highly inefficient, less than 50%; with 10% to 15% of used azo dyes are thus released directly into the environment (Telke

et al., 2008). Similarly, chemicals such as 4-nitrophenol (4-NP) that are increasingly used in the production of herbicides, insecticides, and synthetic dyestuffs are regarded as an environmentally harmful substance (Chen et al., 2018; O'Connor and Young, 1989; Singh et al., 2017; Trapido and Kallas, 2000).

Many conventional methods based on physical/chemical principles are available to treat the contamination of dye. However, the practical use of these methods is generally restricted as their applications are associated with expensive chemicals and/or equipment, complex steps and processes, and production of secondary pollutants (some of which can be more toxic than the primary pollutants) (Nawaz and Ahsan, 2014; Singh and Arora, 2011). Advanced oxidation processes (AOP) are often suggested as a proper means to address some of these limitations.

* Corresponding authors.

E-mail addresses: kkim61@hanyang.ac.kr (K.-H. Kim), jagpreetnano@gmail.com, jagpreetsinghnano@sggswu.edu.in (J. Singh), mohitnano.nit@gmail.com, mohit.rawat@sggswu.org (M. Rawat).

¹ Superscript 1 denotes equal contribution as co-first authors.

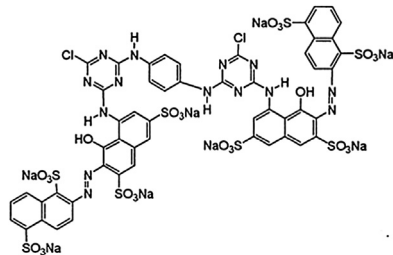
<https://doi.org/10.1016/j.envint.2020.105924>

Received 2 April 2020; Received in revised form 20 June 2020; Accepted 21 June 2020

0160-4120/ © 2020 The Author(s). Published by Elsevier Ltd. This is an open access article under the CC BY license (<http://creativecommons.org/licenses/by/4.0/>).

Table 1

Chemical and structural properties of the target dye studied in this work.

S/N	Dye	CAS registry number	Molecularweight (Da)	Structure
1.	Reactivred-141(RR-141)	61931-52-0	1774.19	

In particular, nanoparticle (NP)-mediated processes based on generation of reactive oxygen species (ROS) in the presence of light (visible, ultraviolet [UV], or both) are highly effective photocatalysts for dye degradation (Ahmed et al., 2017; Baruah et al., 2018; Deng and Zhao, 2015; Trapido and Kallas, 2000; Vieira et al., 2018). However, many NP-based photocatalysts only utilize a limited portion of the solar spectrum. For example, TiO₂ NPs are effective photocatalysts only under UV irradiation. In contrast, silver nanoparticles (AgNPs) are regarded as a highly effective option for photocatalytic treatment as they can accommodate both the UV and visible regions of the electromagnetic spectrum for actual operation (Leong et al., 2018). The utility of AgNPs has further been recognized as catalytic media to treat 4-NP (Mody et al., 2010; Sreekanth et al., 2016; Suchomel et al., 2018). In addition, the utility of AgNP structures has been identified as effective inhibitors for multiple microbial-resistant pathogens (Rolim et al., 2019; Slavin et al., 2017; Wang et al., 2017). As such, AgNPs can be employed based on diverse principles or multiple platforms (as photocatalyst, catalyst, and antimicrobial agent) to remove different types of pollutants such as RR-141, 4-NP, and pathogenic bacteria from aquatic environments, respectively.

Several physical and chemical methods have been explored for the synthesis of AgNPs by employing organic and inorganic stabilizing/capping agents (Reverberi et al., 2016; Van Dong et al., 2012; Wani et al., 2011; Zhang et al., 2016). However, these approaches often use noxious and expensive chemicals, involve complex and/or time-consuming processes, and may generate toxic wastes and by-products. Therefore, the development of an environmentally friendly, renewable, easy-to-implement, and cost-effective means of synthesizing AgNPs has become one of the foremost demands in the field of environmental remediation. AgNPs can be produced through a variety of green synthesis routes if one can effectively utilize the biomolecules (e.g., proteins and vitamins) and phytochemicals (e.g., phenols and flavonoids) within plants (biomass) as natural reducing and capping agents (Raveendran et al., 2003; Singh et al., 2018a; Yadi et al., 2018). This eliminates the need for harmful and expensive chemicals in reduction of metal salts and capping of NPs (as is the case in chemical reduction methods).

Herein, a facile and inexpensive green synthesis method is proposed to prepare highly stable AgNPs with the aid of *Phaseolus vulgaris* seed extract. The produced AgNPs were then employed to investigate their potential as environmental remediation agents (photocatalyst, catalyst and antimicrobial). *P. vulgaris* seeds contain several essential vitamins, proteins, minerals, flavonoids, phenolic compounds, and antioxidants (e.g., lutein, zeaxanthin, and β -carotene) that play important roles in the synthesis of AgNPs (Udani et al., 2018).

To date, only a few studies have been reported to address the utility of *P. vulgaris*, in the synthesis of AgNPs (Deb, 2014; Khandelwal et al., 2020; Paul et al., 2015). However, from almost none of them, the catalytic/photocatalytic potential or stability of the synthesized AgNPs has been assessed in detail at the same time. In this study, the potential of

AgNP as triple remediation platforms for photocatalyst, catalyst, and disinfectant is assessed against RR-141, 4-NP, and *Escherichia coli*/*Bacillus subtilis* bacteria, respectively. Furthermore, studies on the ROS and chemical oxygen demand (COD) were also carried out to support the verification of their remediation potential and recyclability/reusability.

2. Materials and methodology

2.1. Materials

P. Vulgaris seeds were purchased from a local market in Fatehgarh Sahib, Punjab, India, and thoroughly rinsed with distilled water to remove dirt and debris. The bacteria *E. coli* (DH-5 α) and *B. subtilis* were procured from the Department of Biotechnology, SGGSWU, Punjab, India. Silver nitrate (AgNO₃), sodium hydroxide (NaOH), sodium borohydride (NaBH₄), and 4-NP were purchased from Merck, Germany. RR-141 was purchased from Parswanath Dye Stuff Industries, Ahmedabad, India. All glassware was washed with aqua regia (1:3 vol of concentrated HNO₃/HCl) and then rinsed with deionized (DI) water before use.

2.2. Methodology

2.2.1. Synthesis of AgNPs

A mixture of *P. Vulgaris* seeds (10 g) and distilled water (100 mL) was heated at 80 °C for 1 h, followed by filtration. AgNPs were synthesized by adding 1, 2, 3, and 4 mL of the resulting filtrate (extract) into the AgNO₃ solution (0.01 M, 50 mL) and stirred at a constant speed (300 rpm) for 30 min. (The pH of the extract was maintained at 10 using buffer solution to ensure optimal outcomes (Singh et al., 2019)). With time, the color of the solution changed from colorless to light yellow and dark brown, indicative of the reduction of silver ions into AgNPs.

2.2.2. Quantitation of AgNPs

The concentration of AgNPs was estimated from the concentration of AgNO₃ solution (0.01 M, 50 mL) using a procedure described by Kalishwaralal et al. (2010) as follows:

Step 1: Average number of atoms per nanoparticle (N):

(It was assumed that 100% of the silver atoms were converted into silver NPs.)

$$N = \frac{\pi \rho D^3}{6M} N_A$$

where $\pi = 3.14$, ρ is the density of the face-centered cubic crystalline (fcc) structure of silver (i.e., 10.5 g/cm³), D is the average diameter of AgNPs (16 nm), M is the atomic mass of silver (107.86 g), and N_A is the number of atoms per mole (Avogadro's number = 6.023×10^{23}).

Therefore,

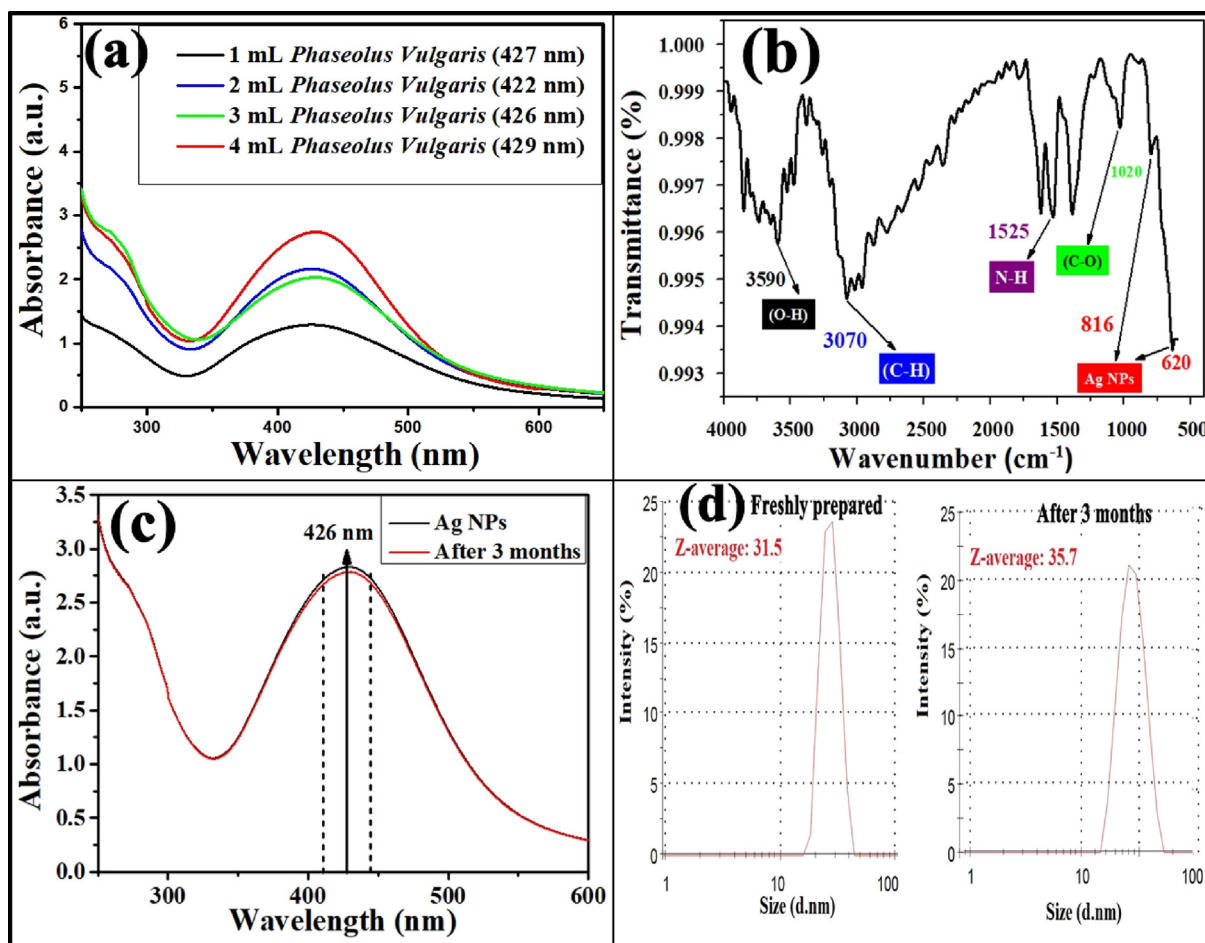


Fig. 1. Optical study of AgNPs: (a) UV–visible spectra of AgNPs prepared using 1–4 mL *P. vulgaris* seed extracts, (b) FTIR spectrum of finally prepared AgNPs, (c) and (d) the UV–visible absorbance and Zetasizer graph, respectively, of freshly prepared AgNPs and 3-month-old AgNPs.

$$N = \frac{3.14 \times 10.5 \times (1.6 \times 10^{-6})^3 \times 6.023 \times 10^{23}}{6 \times 107.86} \quad (1)$$

$$N = 125683$$

Step 2: Molar concentration of AgNPs solution (C):

$$C = \frac{N_T}{NVN_A} \quad (2)$$

where N_T is the total number of silver atoms, which is equal to the molarity of silver nitrate (0.01 M) \times atoms present in one mole (6.023×10^{23}), N is number of atoms per nanoparticle (calculated in step 1), and V is the volume of solution (L).

By putting the value of N obtained from Step 1 into Eq. (2),

$$C = \frac{0.01 \times 6.023 \times 10^{23}}{125682.98 \times 0.05 \times 6.023 \times 10^{23}} \quad (3)$$

$$C = 1.59 \times 10^{-6} \text{ M.L}^{-1} = 1590 \text{ nM}$$

2.2.3. Catalytic activity: Degradation of 4-NP

The addition of AgNPs (1590 nM) were made at three different volumes (e.g., 10, 20, and 30 μL) to an aqueous solution made of 4-NP (40 μL , 5×10^{-2} M), DI water (1.65 mL), and NaBH_4 (200 μL , 2×10^{-1} M). The progress of the reaction was monitored by UV–vis spectroscopy after every 3 mins until no further significant change takes place.

2.2.4. Photocatalytic activity: Degradation of RR-141

An aqueous solution of RR-141 (50 mL, 20 ppm) was allowed to equilibrate at room temperature (in dark condition over 30 min). Thereafter, the as synthesised AgNP (5 mg) was added and stirred

(magnetic stirrer, 200 rpm) for 20 min. The solution was then directly exposed to sunlight. Following exposure, the AgNPs were separated from the dye solution through centrifugation (at 10,000 rpm for 15 min), and the UV–Vis spectrum of the supernatant (2 mL) was recorded. The degradation efficiency (R) was estimated by equations (4) (Gautam et al., 2016):

$$R = \{(C_0 - C)/C_0\} \times 100 = \{(A_0 - A)/A_0\} \times 100 \quad (4)$$

where C_0/C and A_0/A represent the concentration and absorbance of dyes, respectively, at time $t = 0/t$.

The quantum efficiency (QE) of the removal process was also calculated by:

$$QE = \frac{\text{no. of degraded dye molecules}}{\text{no. of photons absorbed}} \quad (5)$$

2.2.5. Complete mineralization evaluation and reactive oxygen species (ROS) assessment

The complete mineralization of the dye was determined by monitoring the reduction in COD. For this purpose, 2 mL of test solution was pipetted into the standard amount of potassium dichromate and kept at 150 $^\circ\text{C}$ for 2 h. Then, COD was estimated on COD meter (Bansal and Sud, 2012).

A scavenger experiment was undertaken to investigate the ROS in photocatalysis. In this regard, different quenchers (with concentration 0.5 mM) were used such as: (i) methanol for hydroxy radical (OH^\cdot), (ii) p-benzoquinone (p-BQ) for superoxide radicals (O_2^\cdot), and (iii) ammonium oxalate (AO) for holes (h^+). (Mavai et al., 2020; Suliman et al.,

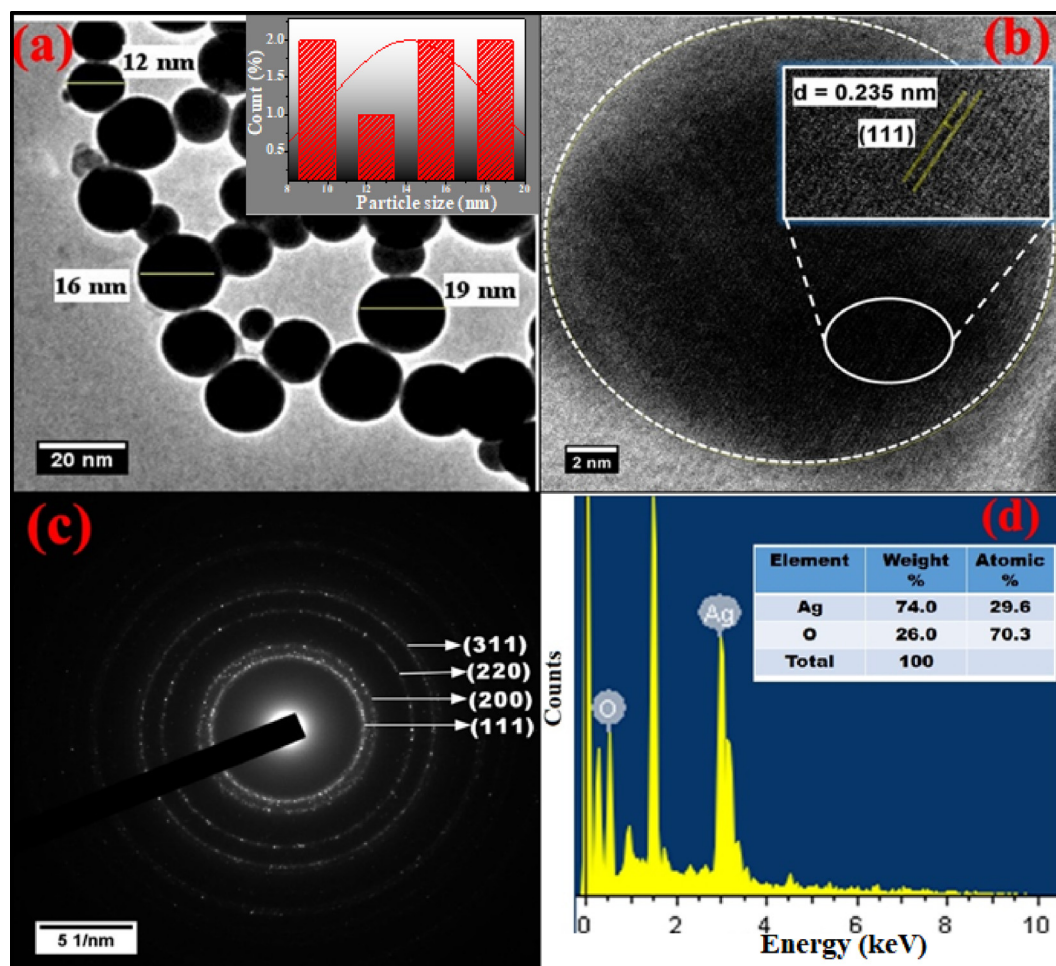


Fig. 2. Microscopic study: (a-b) HR-TEM micrographs of AgNPs (inset shows the particle size distribution curve and interplanar d-spacing, respectively); (c-d) SAED and EDX pattern of AgNPs, which illustrate its crystal planes and elementary composition, respectively.

Table 2

Interplanar d-spacing and corresponding lattice planes calculated from SAED patterns.

S/N	2R	R [1/nm]	R [nm]	R [Å]	Lattice plane
1.	8.17	4.08	0.24	2.44	(111)
2.	9.54	4.77	0.20	2.09	(200)
3.	13.54	6.77	0.14	1.47	(220)
4.	15.94	7.97	0.12	1.26	(311)

2019). After adding these scavengers with AgNPs, photocatalytic activity was monitored under the same reaction conditions described above.

2.2.6. Assessment of antimicrobial activity

A conventional well-plate diffusion technique was used to evaluate the antibacterial potential of the as-synthesized AgNPs. First, bacterial cultures were grown in Luria broth (LB) overnight and then incubated in LB at 37 °C. Subsequently, wells were punched in the LB plates. The prepared AgNPs were then added into the wells at different volumes (20, 40, 60, and 80 µL) and placed at 37 °C for one day.

2.2.7. Characterization of AgNPs

An optical study of synthesized AgNPs was undertaken using a Shimadzu-UV 2600 spectrophotometer at wavelengths from 200 to 800 nm. The role of biomolecules in the extract and their interaction with AgNPs were investigated by an Alpha Fourier-transform infrared

(FTIR) spectrophotometer (Bruker Corp.). The average particle size was estimated by a particle-size analyzer (Malvern-ZEN-1690). Morphological characteristics and accurate particle sizes were measured from high-resolution transmission electron microscope (HR-TEM; Jeol JEM-2100) images. Similarly, the crystalline structure and interplanar d-spacing between lattice planes were estimated using selected area electron diffraction (SAED). The quantitative stoichiometric configuration of the prepared sample was determined by energy-dispersive X-ray spectroscopy on an Oxford Instruments X-Max 51 –XMX0004.

3. Results and discussion

3.1. Characterization of synthesized AgNPs

Addition of the 1, 2, 3, and 4 mL of *P. vulgaris* seed extract to AgNO₃ solution at room temperature changed the appearance of the solution from colorless to pale yellow and finally to a dark brownish-red color. The latter is indicative of the formation of AgNPs through the reduction of Ag⁺ ions to Ag⁰ (Li et al., 2007) as also evidenced by UV–visible spectroscopy (Fig. 1a). A sharp band between 420 and 430 nm was observed to commensurate with surface plasmon excitations. At 2 mL of extract, observations of a blue shift (at 422 nm) confirmed the narrow size distribution of AgNPs (Jain and Mehata, 2017). It was suspected that large amount of reductive phytoconstituents led to a rapid formation of Ag NPs followed by their subsequent growth via Ostwald reopening. Therefore, the size of NPs will increase over time to cause red shift in UV spectrum (Shaik et al., 2018). In the present case, the

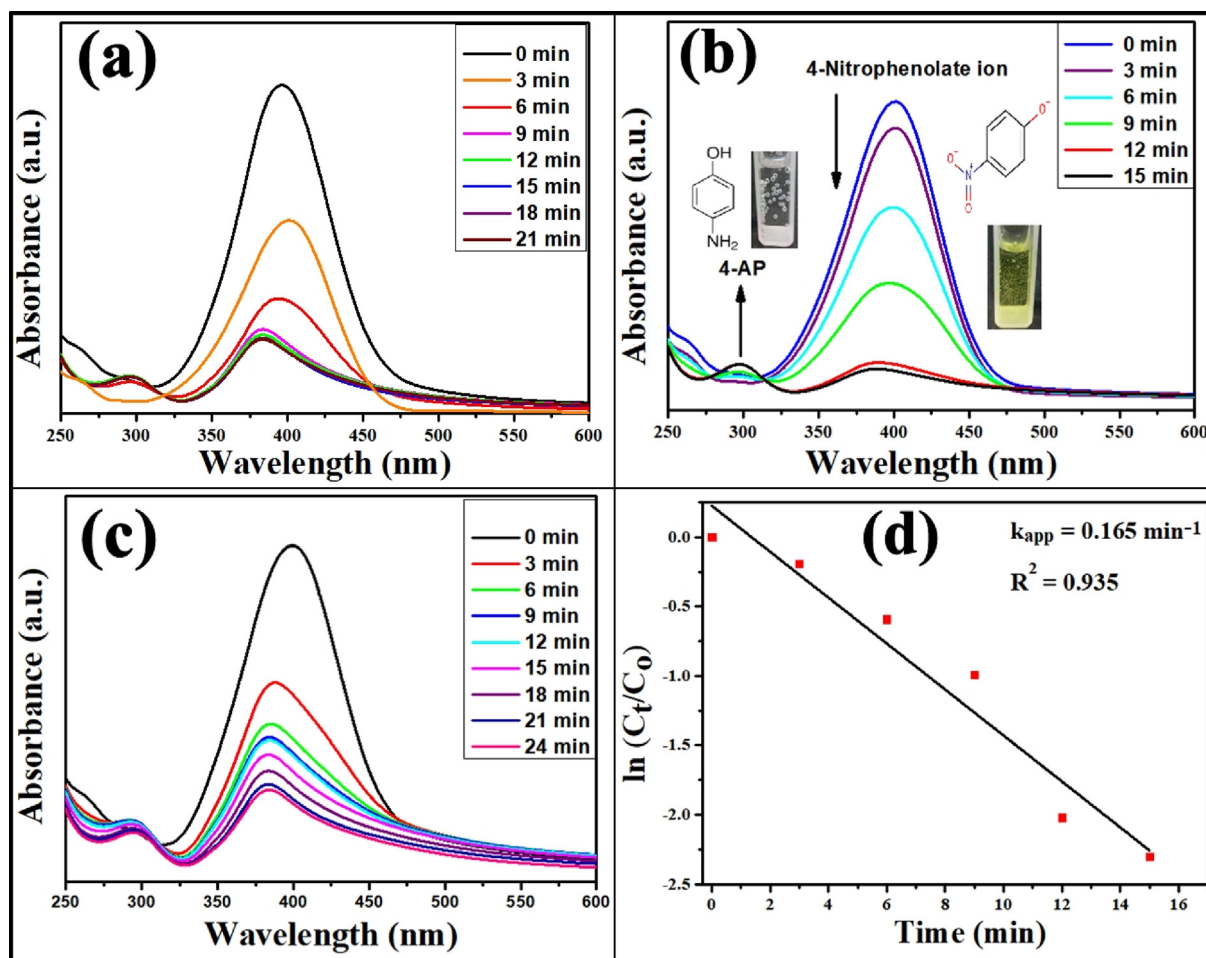


Fig. 3. Catalytic study: (a-c) UV-visible spectra illustrating AgNP (10, 20, and 30 μL)-mediated catalytic reduction of 4-NP to 4-AP and (d) kinetic study of catalytic reduction.

2 mL volume of extract was treated as an optimal volume for the preparation of AgNPs. Hence, AgNPs prepared through this route were used for further characterization and degradation studies.

The functionality present on AgNP surfaces was investigated by FTIR spectroscopy. Fig. 1(b) shows the FTIR spectrum of the as-synthesised AgNPs. Strong absorption bands at 3590 (O-H str.), and 3070 cm^{-1} (C-H str.), 1670 cm^{-1} (C = O str.), and 1525 cm^{-1} (N-H bend, Amide I) are indicative of organic or proteinaceous matter on the surface of AgNPs. The proteinaceous matter acts to cap the AgNPs while preventing agglomeration. (Jyoti et al., 2016; Huang et al., 2007). The absorption bands at 816 and 630 cm^{-1} are attributed to the stretching vibrations of AgNPs (Khan et al., 2013). The stability and longevity of the AgNPs were assessed by recording their UV-vis spectrum after three months storage (Fig. 1 d). A very minor decline in absorbance (without any shift in the absorption band) of synthesized AgNPs was noted, signifying the exceptional stability of AgNPs over extended periods. Likewise, the average particle size (Fig. 1.d) showed a very minor increase, i.e., Z-direction from 31.5 to 35.7 nm).

The size and morphology of the as-prepared AgNPs by *P. vulgaris* seeds extract were determined by HR-TEM micrographs (Fig. 2). The synthesized AgNPs exhibited a spherical morphology, ranging in size from 10 to 20 nm (average size ~ 16 nm). As shown in Fig. 2(b), the interplanar d-spacing between the lattice fringes was 0.235 nm, corresponding to the (111) lattice plane. The identification of a crystalline structure was investigated by SAED analysis, as shown in Fig. 2(c). The bright circles confirmed the polycrystalline nature of the AgNPs. From the SAED pattern, the interplanar d-spacings were estimated to be 2.44, 2.09, 1.47, and 1.26 Å, corresponding to the (111), (200), (220), and

(311) lattice planes, respectively, as summarized in Table 2. These results resemble the standard data of a crystal structure (JCPDS file no. 00-004-0783) to support the (fcc) crystal structure of our as-synthesized AgNPs. The surface elemental composition of AgNPs (Fig. 2(d)) showed the predominance of Ag (74%) and O (26%) on mass basis. (Note that only % elemental values of Ag and O was considered in present case.) The presence of oxygen correlates well with FTIR data (O-H str.) and our premise that organic molecules, e.g. proteinaceous matter should be involved in capping of the AgNPs (Jyoti et al., 2016).

3.2. Catalytic activity of synthesized AgNPs

Due to the well-known catalytic properties of AgNPs, they are considered effective catalysts for the degradation of harmful dyes. The catalytic performance of synthesized AgNPs was analyzed by evaluating the reduction and degradation of 4-NP and RR-141, respectively. These performance parameters were evaluated by recording the time-dependent UV-visible spectra of both molecules. In the reduction of 4-NP, a sharp absorption band was evident at 315 nm (Fig. S1). After the addition of sodium borohydride and AgNPs into the reaction medium, 4-NP is initially converted into its nitrophenolate intermediate (evidenced at 400 nm) (Fig. S1), followed reduction to 4-aminophenol. This change is reflected by the appearance of a new band in the UV-visible spectrum at 296 nm (Kästner and Thünemann, 2016). As the reaction proceeds, the intensity of the 400 nm peak decreases, whilst the intensity of the 296 nm peak increase. The effect of amount of AgNPs on the catalytic reaction was also investigated. As shown in Fig. 3(a-c), the reduction of 4-NP was tested using three volumes (10, 20, and 30 μL) of

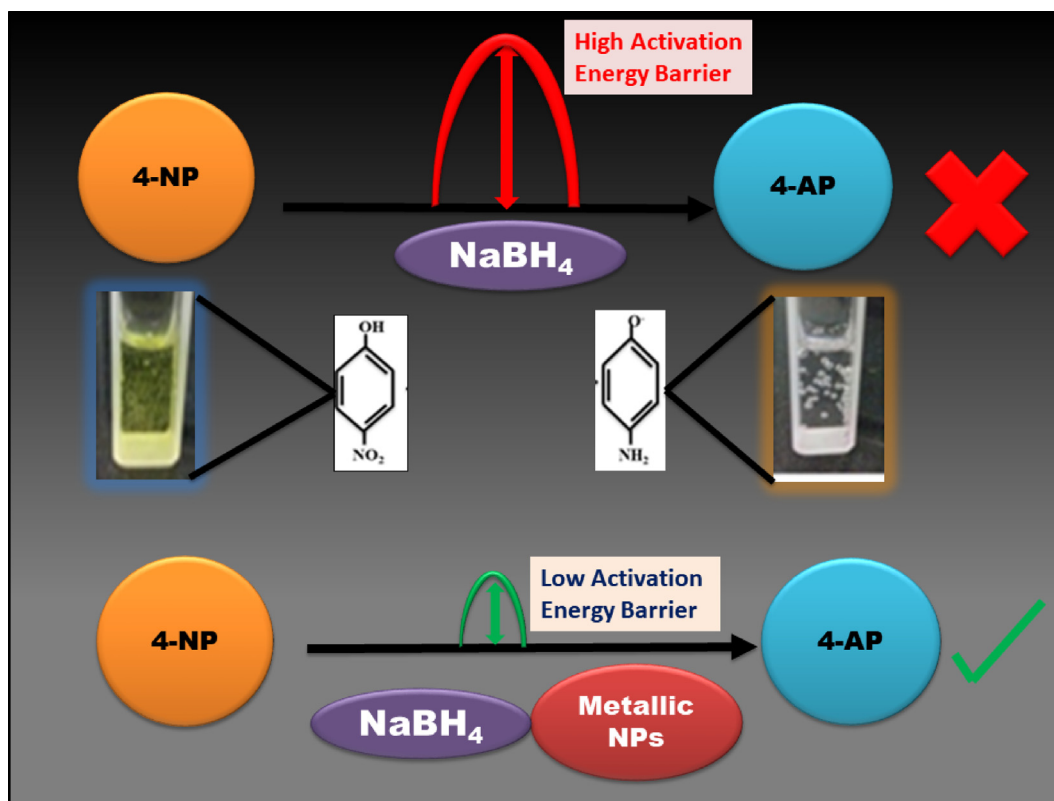


Fig. 4. Schematic shows the proposed mechanism of 4-NP reduction by *Phaseolus vulgaris*-mediated AgNPs.

Table 3

Performance comparison of silver nanoparticles and their composites for catalytic reduction of 4-NP to 4-AP.

S/N	Catalyst	Synthesis method	Concentration of 4-nitrophenol(g/L)	Catalyst loading (mg/mL)	Reaction time (min)	Kinetic rate (mmol/g/h)	References
1	Ag/PAN CFNs	Hydrothermal	0.01	0.33	70	0.185	(Gao et al., 2016)
2	Ag-P(NIPAM-co-AAm)	Precipitation polymerization	0.008	23.90	25	—	(Begum et al., 2016)
3	AgNP-enriched SiO ₂	Green (seed mediated)	0.06	0.25	26	—	(Online and Lee, 2015)
4	CNC/CTAB/Ag nanohybrid composite	Hydrolysis	0.01	—	20	—	(An et al., 2016)
5	AgNPs	Green (using curcumin)	0.18	21.6	20	0.186	(Verma et al., 2016)
6	AgNPs/PD/ PANFP	Wet chemical	0.01	—	30	—	(Lu et al., 2017)
7	AgNPs/polymer nanofiber	Wet chemical	2.78	0.2	30	3.996	(Xiao et al., 2012)
8	AgNPs	Green(leaves of <i>C. occidentalis</i>)	0.02	0.1	30	0.003	(Gondwal and Joshi Nee Pant, 2018)
9	Biogenic AgNPs	Green (kidney beans)	0.69	0.0001	15	1.587	This study

AgNP solution prepared at 535 nM. Accordingly, 20 μL of AgNPs achieved the maximum reduction of 4-NP. With 20 μL of AgNPs, complete degradation of 4-NP took 15 min. The results with 10 and 30 μL took comparatively longer 21 and 24 min, respectively. We therefore concluded that 20 μL of AgNPs was optimal for the 4-NP catalytic performances. This may be due to an increase in amounts of catalyst and capping agents (phytoconstituents), which slowed the reaction rate. As reported previously, the increasing the amount of plant extract and capping agents reduced the reaction rate by slowing re-structuration (involving redox reactions between reactants and catalyst) on the surface of the catalyst (Bingwa and Meijboom, 2014; Niu and Li, 2014). In a control sample, the reduction of 4-NP was negligible in the absence of AgNPs (Fig. S2).

The kinetics of the catalytic reaction was determined by plotting a graph of normalized concentration (C_t/C_0) versus time. Fig. 3(d) shows that the 4-NP reduction using AgNPs was well fit by a pseudo-first-order rate equation. The apparent rate constant (K_{app}) of 4-NP reduction was estimated using a pseudo-first-order rate equation (Thawarkar et al.,

2018):

$$\ln(C_t/C_0) = -k_{app} \cdot t \quad (6)$$

where C_t and C_0 are concentrations of the reactant (4-NP) at times $t = t$ and $t = 0$, respectively (Singh et al., 2018b). The K_{app} value for 20 μL of AgNPs was calculated to be 0.165 min^{-1} with correlation coefficient (R^2) of 0.935. It can thus be inferred that the catalytic reaction should follow the pseudo first order kinetic rate. The kinetic rate of this reaction was estimated to be $1.59 \text{ mmol g}^{-1} \text{ h}^{-1}$. The high surface-to-volume ratio and active surface sites of AgNPs are speculated to reduce the activation energy barrier between 4-NP and 4-AP. These properties of AgNPs were reported to facilitate the catalytic conversion of 4-NP into 4-AP at ultra-high speed (Zhao et al., 2015).

A proposed mechanism for 4-NP catalytic reduction is described in Fig. 4. In the first step, the addition of sodium borohydride leads to conversion of 4-NP to nitrophenolate ion. As there is a large potential difference between acceptor (4-NP = 0.76 V) and donor molecules ($\text{BH}_4 = 1.33 \text{ V}$), a large activation energy barrier is created. However,

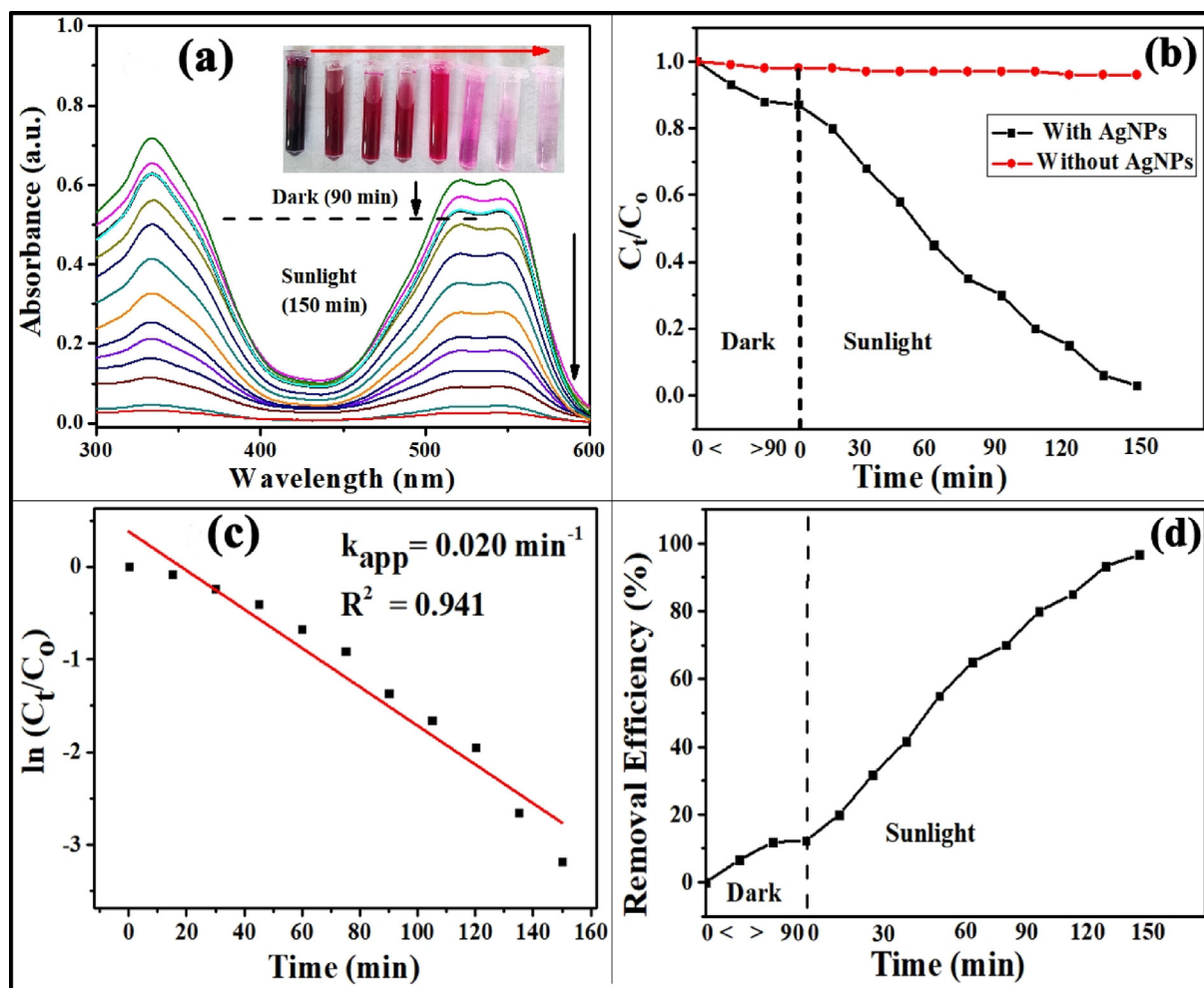


Fig. 5. Dye degradation study: (a) UV-vis graphs of Reactive Red 141 (RR-141) dye in a time bound study, (b) normalized absorbance of dye in dark and sunlight in the presence and absence of catalyst, (c) kinetic study of dye degradation, and (d) dye removal efficiency with reaction time. (For interpretation of the references to color in this figure legend, the reader is referred to the web version of this article.)

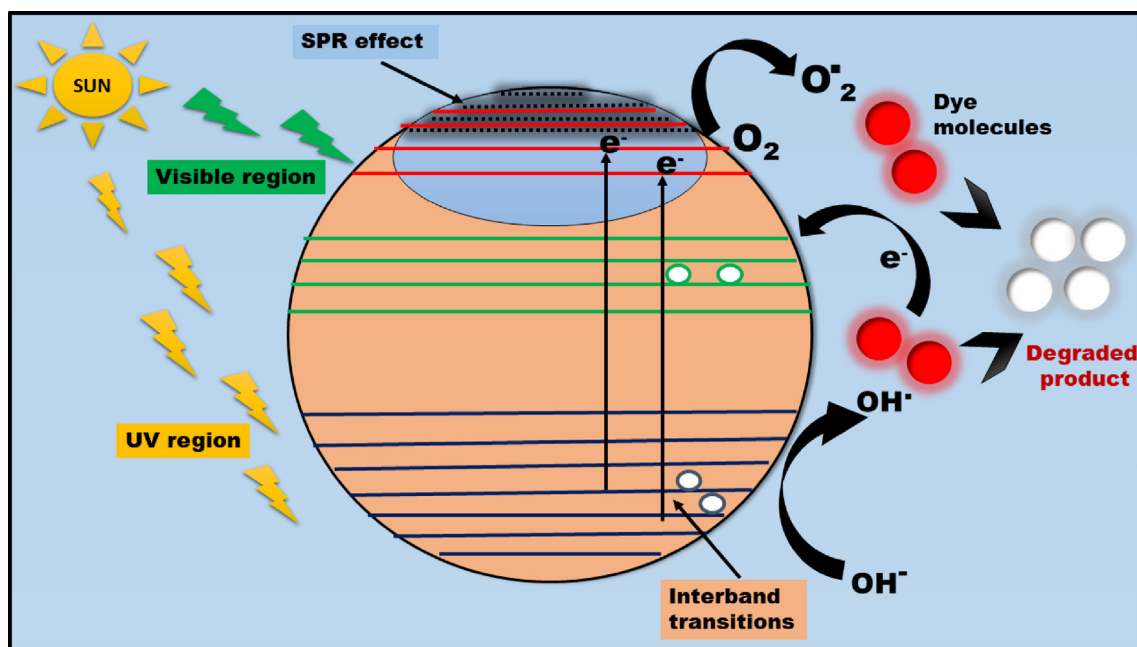


Fig. 6. Schematic shows the mechanistic processes in AgNP-based photocatalytic degradation of Reactive Red 141 dye. (For interpretation of the references to color in this figure legend, the reader is referred to the web version of this article.)

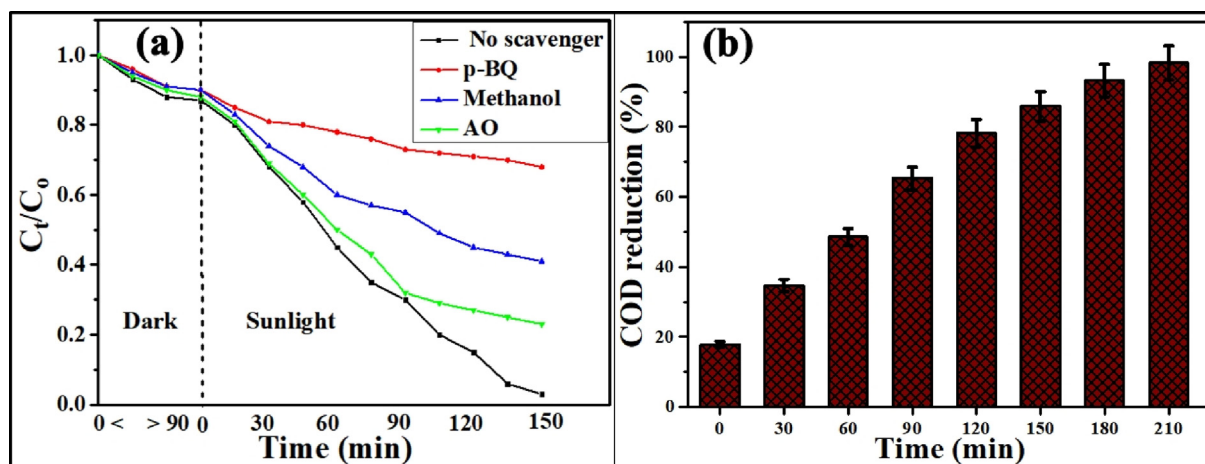


Fig. 7. Photocatalytic processes: (a) Trapping of ROS using methanol, p-benzoquinone (p-BQ), ammonium oxalate (AO) for hydroxy radical (OH^\bullet) and superoxide radicals (O_2^\bullet), and holes (h^+) respectively, and (b) bar graph of COD reduction indicates the complete mineralization of dye.

AgNPs efficiently reduce the activation energy barrier (acting as electron reservoir (between donor and acceptor molecules) known as electron relay effect) to convert 4-nitrophenolate ion into 4-aminophenol. Table 3 compares the performance of different catalytic systems for reduction of 4-NP to 4-AP. Previous efforts employed silver-based nanocomposites through complex chemical processes such as precipitation polymerization, hydrolysis, and hydrothermal synthesis. In contrast, in the present study, a simpler and more environmentally friendly system is developed for efficient reduction of 4-NP.

3.3. Photocatalytic performance of AgNPs

The photocatalytic degradation of RR-141 dye in the presence of AgNPs was monitored by UV-vis spectroscopy (absorption bands at 534 and 332 nm, see Fig. 5(a)). Upon addition of AgNPs and exposure to sunlight, the intensity of these absorption bands started to decrease, as shown in Fig. 5(a). The average sunlight flux was estimated on the pyranometer as 645 W/m^2 .

A control experiment with and without catalyst in dark and sunlight environments was also performed to determine the effects of catalyst and sunlight alone. In the absence of catalyst, a negligible decline in RR-141 absorbance was observed in both the dark and sunlight. Likewise, when the dye degradation experiment was conducted in the dark in the presence of a catalyst, a minor decline in absorbance was observed (Fig. 5(b and d)). These results suggest that the progress of dye degradation should rely on both AgNPs and sunlight. A kinetic study revealed the photocatalytic reaction to have a pseudo-first-order relationship, with an apparent rate constant (k_{app}) and R^2 of 0.02 min^{-1} and 0.941, respectively, as shown in Fig. 5(c). Nonetheless, due to the high molecular weight (1774.19 g/mol), low diffusion rate, and complex structure (two azo groups), RR-141 was not as easily degraded compared with the lab dyes (methylene blue: 319.85 g/mol ; Congo red: 696.66 g/mol) (Jagade et al., 2012; Khataee and Kasiri, 2010; Muhd Julkapli et al., 2014). The dye degradation efficiency was approximately 97% within 150 min. Moreover, the QE of the photocatalytic process was $3.68 \times 10^{-6} \text{ molecule.photon}^{-1}$, with a removal rate of $3.66 \times 10^{13} \text{ molecule.sec}^{-1}$ and kinetic rate was estimated to be $1.13 \times 10^{-2} \text{ mmol.g}^{-1}\text{h}^{-1}$.

The dye degradation mechanism by AgNPs is based on plasmon-derived photocatalysis. One of the advantages of using AgNPs as photocatalysts is that they can utilize both the visible and UV regions of the solar spectrum due to surface plasmon resonance and their inter-band transition properties. The excitation of sp-band electrons of AgNPs involves absorption of light in the visible region. The plasmon effect produces heat energy or hot electrons, which interact with oxygen and

generate oxygen free radicals (e.g., O_2^\bullet). These energetic free radicals are responsible for degradation of dye molecules. The holes generated in the 5 sp band can enhance degradation performance by acquiring electrons from dye molecules. Similarly, under UV radiation exposure (from sunlight), inter-band transitions took place in the 4d orbital of the AgNPs. This process generated highly energetic oxygen and hydroxy radicals (O_2^\bullet , OH^\bullet), which degraded dye molecules. (Kale et al., 2014; Kumar et al., 2013; Leong et al., 2018; Roy et al., 2015a, 2015b; Sumi et al., 2017). The dye degradation mechanism is illustrated in Fig. 6. Furthermore, a scavenger experiment was carried out to determine the role of specific ROS species in the photocatalytic process. As seen in Fig. 7(a), the photocatalytic activity was greatly affected and declined relative to the control when p-BQ and methanol were present as scavengers. Also, a minor decline was observed when AO was employed as a scavenger. Therefore, it can be inferred that the superoxide (O_2^\bullet), and hydroxyl (OH^\bullet) radicals are the dominant ROS species in the photocatalytic activity of AgNPs. In other words, the relative dominance of ROS species in the photocatalytic process can be estimated as $\text{O}_2^\bullet > \text{OH}^\bullet > \text{h}^+$.

The complete mineralization was also estimated by evaluating the reduction in COD as shown in Fig. 7(b). The complete mineralization of dye took longer (e.g., 60 min) than photocatalytic degradation. This might be due to the formation of some intermediate (uncoloured) moieties that can intervene in the degradation process (Bansal and Sud, 2012).

To validate the efficacy of photocatalytic activity of AgNPs observed in this work relative to the finding of other studies, all related data were surveyed as described in Table 4. We also estimated the QE of all relevant studies. In most of previous studies on AgNPs with a variety of forms (composites, core-shell, etc.), the efficiency of the photocatalytic process was estimated under highly favorable conditions (e.g., use of artificially intense light sources and lab dyes (highly degradable component with low molecular weight and high diffusion rate)). In comparison, the present AgNPs system was demonstrated to have appreciable photocatalytic potency (as seen from QE values) without such adjustment for favorable experimental conditions. It can thus be inferred that the developed system can be employed to effectively destroy hard-to-degrade reactive dyes.

The re-usability and recyclability of the as-synthesised AgNPs were also tested for catalytic (reduction of 4-NP) and photocatalytic applications (degradation of RR-141) as shown in Fig. 8. The as-synthesised AgNPs showed excellent recyclability and efficacy with up to 5 time re-use. Only, a minor decline in catalytic and photocatalytic activity of AgNPs was observed even after five runs.

Table 4
Performance comparison of silver nanoparticles and their composites for degradation of various pollutant dyes.

S/N	Catalyst	Method of synthesis	Dye	Concentration of dye(g/L)	Catalyst loading(mg/mL)	Light source/irradiation/wavelength (nm)	Reactiontime (min)	Degradation efficiency (%)	Kinetic rate (mmol/g/h)	Quantum efficiency (QE) (molecule photon ⁻¹)	Ref.
1	Ag-SnO ₂	Sol-gel	Methylene blue	0.006	1	Hg lamp/254 nm	120	90	—	—	(Ahmed et al., 2017)
2	Ag-TiO ₂	Electro-chemical	Methyl orange	0.02	0.5	Hg lamp/365 nm	120	98.5	4.57×10^{-2}	3.42×10^{-7}	(Petica et al., 2019)
3	AgNPs	Green using <i>Parkia speciosa</i> leaf extract	Methylene blue	0.001	0.1	Sunlight	180	84	—	—	(Ravichandran et al., 2019)
4	Ag-ZrO ₂	Solution phase reduction	Sulfo-rhodamine-B	0.001	1	UV tube light/450 nm	240	66	2.48×10^{-3}	1.01×10^{-7}	(Chen et al., 2010)
5	Ag-TiO ₂ P25 hybrid	Dip coating	Methyl orange	175.16	0.02	UV-C lamp/253.7 nm	150	45	1.0×10^1	5.90×10^{-1}	(Kodom et al., 2015)
6	AgNPs	Green using <i>Shorea robusta</i> extract	Rhodamine B	0.02	0.01	UV chamber/*365 nm	120	77.4	1.04×10^{-4}	3.35×10^{-6}	(Shaikh et al., 2019)
7	AgNPs	Green using <i>Z. armatum</i> leaf extract	Methylene blue	0.01	0.1	—	1,440	—	—	—	(Jyoti and Singh, 2016)
8	Ag- Halloysite	Chemical reduction	Safranin O	0.001	0.1	—	1,440	—	—	—	(Fatimah and Herianto, 2018)
9	Ag- Halloysite	Chemical reduction	Rhodamine B	0.02	—	UV lamp/*365 nm	120	—	—	—	(Mohan and Devan, 2019)
10	Ag-Ni bimetallic NPs	Green using zinger extract	Saffranin O	0.01	0.2	Hg lamp/*365 nm	25	62.5	3.48×10^{-1}	1.32×10^{-6}	(Roy et al., 2015c)
11	AgNPs	Green using potato leaves	Methyl orange	0.01	1	Sunlight	480	75	—	—	(Wang et al., 2018)
12	AgNPs	Green using <i>Psidium guajava</i> leaves	Methyl orange	0.01	0.4	UV light tubes/450 nm	600	~ 60	—	—	(Kumari et al., n.d.)
13	AgNPs	Green using <i>Cordia dichotoma</i> leaf extract	CBB G 250	0.01	0.4	Sunlight	300	~ 70	—	—	(Fageria et al., 2014)
14	AgNPs	Green using <i>Cordia dichotoma</i> leaf extract	Methylene blue	0.01	0.5	Sunlight	360	—	—	—	(Sinha and Ahmaruzzaman, 2015)
15	ZnO/Ag nano-flower	Surfactant-mediated	Methylene blue	0.015	2.5	Tungsten lamp/365 nm	120	40	1.99×10^{-3}	6.04×10^{-8}	(Mariselvam et al., 2016)
16	Au-Ag core shell NPs	Green using eggshell	Methyl violet 6B	3.93	0.05	Sunlight	150	97.6	—	—	(Zhang et al., 2018)
17	AgNPs	Green using coconut tree	Azo dye	—	—	Sunlight	240	—	—	—	(Khanna and More, 2018)
18	Ag-TiO ₂	Hydro-thermal gel	Methyl orange	0.02	1	Hg lamp/365 nm	180	79.4	1.90×10^{-2}	6.89×10^{-6}	(Saeed et al., 2019)
19	AgNPs	Chemical reduction	Methylene blue	0.05	1	UV lamp/365 nm	240	28	3.91×10^{-2}	2.49×10^{-6}	(Subash et al., 2013)
20	Ag-TiO ₂	Green using <i>Azadirachta indica</i> leaves	Rhodamine B	0.1	2	UV light/*365 nm	120	90	—	—	(Raj Pant et al., 2013)
21	Ag-ZnO	Precipitation–thermal decomposition method	Reactive red 120	—	—	Sunlight	30	—	—	6.9×10^{-3} 2.3×10^{-2}	(Khanna and Shetty, 2014)
22	Ag-ZnO/RGO	Hydrothermal method	Reactive black 5	0.01	0.66	Hg lamp/*365 nm	200	~88 ~70	4.59×10^{-3} 4.59×10^{-3}	3.34×10^{-6} 2.66×10^{-6}	(Yola et al., 2013)
23	Ag doped (LI)-CSTiO ₂	Chemical	Reactive blue 220	0.05	1	UV lamp/365 nm	240	~ 32	2.0×10^{-3}	1.67×10^{-6}	(Gunasekar et al., 2013)
24	Ag doped (PD)-CSTiO ₂	Chemical	Reactive blue 220	0.05	1	UV lamp/365 nm	240	~ 40	2.0×10^{-3}	2.02×10^{-6}	(Vanaamudan et al., 2016)
25	Ag doped-SGTiO ₂	Chemical	Reactive blue 220	0.05	1	UV lamp/365 nm	240	~ 68	2.0×10^{-3}	3.44×10^{-6}	
26	Ag@TiO ₂ core shell	Chemical	Reactive blue 220	0.05	1	Sunlight	60	99	1.6×10^{-2}	—	
27	Ag-colemanite ore	Chemical	Reactive blue 220	0.05	1	UV lamp/365 nm	240	98.9	2.0×10^{-3}	5.0×10^{-6}	
28	Ag-colemanite ore	Chemical	Reactive yellow 86	1	1	UV-Vis lamp/250 nm	110	97.7	9.32×10^{-1}	1.49×10^{-5}	
29	Ag-TiO ₂	Enzyme mediated	Reactive red 2	1	1	Sunlight	110	95.2	9.03×10^{-1}	1.41×10^{-5}	
30	Ag-TiO ₂ biotemplate	Enzyme mediated	Reactive black b	0.1	1	Sunlight	80	92	7.76×10^{-2}	—	
31	AgNPs	Green using palm shell	Reactive red 141	0.1	0.16	—	210	—	—	—	

(continued on next page)

Table 4 (continued)

S/N	Catalyst	Method of synthesis	Dye	Concentration of dye(g/L)	Catalyst loading(mg/mL)	Light source/irradiation/wavelength (nm)	Reactiontime (min)	Degradation efficiency (%)	Kinetic rate (mmol/g/h)	Quantum efficiency (QE) (molecule photon ⁻¹)	Ref.
25	AgNPs	Green using kidney bean extract	Reactive red 141	0.02 (or 20 ppm)	0.1	Sunlight	150	97	1.13×10^{-2}	3.68×10^{-6}	This study

* If wavelength information was not available or provided in the literature, the following values were assumed: UVC = 250 nm, UV = 365 nm, and VIS = 420 nm.

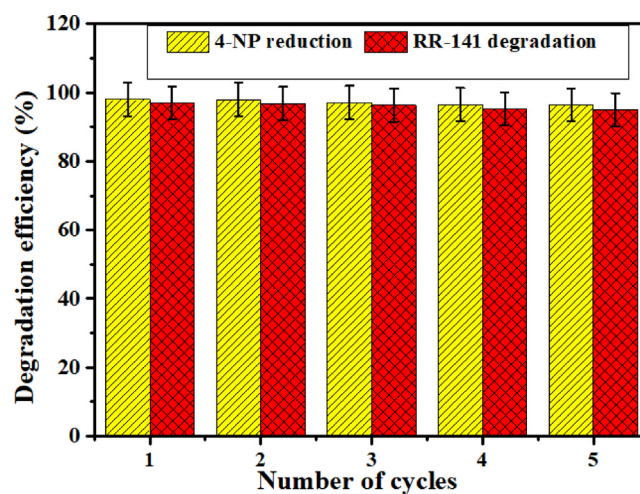


Fig. 8. Reusability test: Degradation efficiency of 4-NP and RR-141 using AgNPs after various test cycles.

3.4. Antibacterial performance of AgNPs

The antibacterial properties of synthesized AgNPs were investigated against two types of bacteria: *E. coli* (gram-negative) and *B. subtilis* (gram-positive). Different volumes of AgNPs were poured into cultured *E. coli* and *B. subtilis* plates by the disk-diffusion method, as presented in Fig. 9 (a and c). Agar plates b and d were designed as controls for *E. coli* and *B. subtilis*, respectively, by adding water, AgNO₃, and *P. vulgaris* extract to the three wells. The four wells in the plate were filled with 20, 40, 60, and 80 µL suspension of AgNPs and labelled as 1, 2, 3, and 4, respectively, in the a and c agar plates.

Different zones of clearance were observed in all the AgNP-treated wells, while no such zones were observed in control plates. The zone of clearance revealed a linear increment in the volume of AgNPs (Fig. 9 and Table 5). It was observed that the synthesized AgNPs showed higher antimicrobial activity towards gram-negative bacteria. This difference may be explained from a number of respects. Firstly, differences in cell wall construction should be considered between the two types of bacteria. As gram-positive bacteria have a thicker cell wall to contain peptidoglycan proteins, they can render resistance to AgNPs relative to the gram-negative bacteria with thinner cell wall. Secondly, it should be noted that the cell wall of gram-positive bacteria is negatively charged. As they can attract silver ions to the surface, it is possible to suppress their amount reaching the plasma membrane (Peiris et al., 2018). Antimicrobial screening analysis confirmed that the biogenic AgNPs possess efficient antimicrobial potential against *E. coli* and *B. subtilis* bacteria. It is suggested that, due to the small size and large intake of AgNPs by bacteria, the AgNPs demonstrated enhanced toxicity toward bacterial strains (Dakshayani et al., 2019; Pirtarighat et al., 2019). The main reason for high antimicrobial activity of AgNPs is production of ROS, which is suspected to be the main factor in bacterial cell death (Lee et al., 2019), along with formation of Ag⁺ (Al-Sharqi et al., 2019). Earlier studies on AgNP antimicrobial activity suggested that these NPs should attack bacterial cells through oxidative stress, DNA damage, protein denaturation, and rupture of the cell transport membrane (Roy et al., 2019). Multiple antimicrobial mechanisms of AgNPs are described in Fig. 10. (Behravan et al., 2019). AgNPs synthesized in an environmentally friendly manner are associated with more effective antimicrobial activity due to the presence of biomolecules compared with commercially available or chemically synthesized NPs (Bagherzade et al., 2017).

4. Conclusions

In this research, a highly stable AgNPs were prepared through an

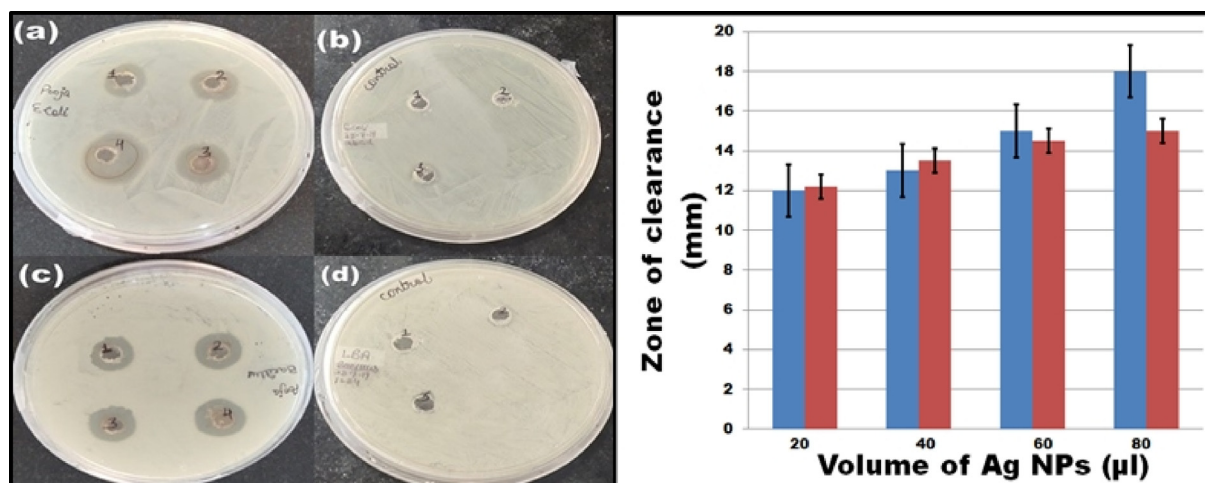


Fig. 9. Left side: Agar plates showing diameters of zones of clearance of *Escherichia coli* and *Bacillus subtilis* treatment with AgNPs (a, c) and with control (b, d), respectively. Right side: Histogram shows that antimicrobial activity of the AgNPs increased linearly with increase in volume of NPs (Blue: *Escherichia coli*; Brown: *Bacillus subtilis*). (For interpretation of the references to color in this figure legend, the reader is referred to the web version of this article.)

Table 5

Zone of clearance with respect to amount of AgNPs.

S/N	Amount of AgNPs (μL)	Zone of clearance (mm)	
		<i>Escherichia coli</i>	<i>Bacillus subtilis</i>
1.	20	12	12.2
2.	40	13.1	13.5
3.	60	15	14.5
4.	80	18	15

environmentally friendly and cost-effective green synthesis approach using *P. vulgaris* seed extract as capping and reducing agent. The triple role (as catalyst, photocatalyst, and antimicrobial agent) of the produced AgNPs was demonstrated based on their efficacy toward the reduction of each selected target such as 4-NP to 4-AP, RR-141, and both gram-positive/-negative bacteria (*Escherichia coli* (achieving an 18 mm maximum zone of clearance) and *Bacillus subtilis* (15 mm maximum zone of clearance)), respectively. Moreover, the as-synthesised AgNPs recorded remarkable stability after various test cycles for catalyst/photocatalyst. This work fosters the possible development of a three-in-one platform for the environmental remediation of waste water systems.

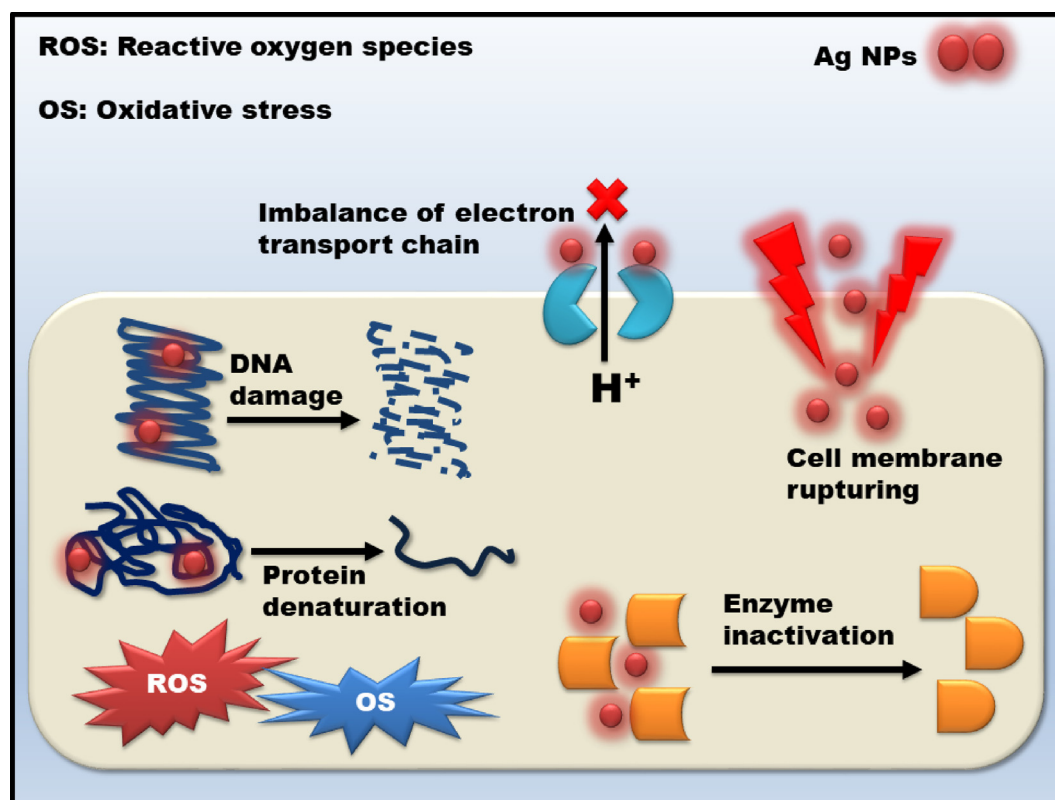


Fig. 10. Schematic shows the multiple antimicrobial mechanism of AgNPs.

CRediT authorship contribution statement

Pooja Rani: Methodology, Writing - original draft. **Vanish Kumar:** Formal analysis, Investigation. **Prit Pal Singh:** Formal analysis, Investigation. **Avtar Singh Matharu:** Formal analysis, Investigation. **Wei Zhang:** Formal analysis, Investigation. **Ki-Hyun Kim:** Funding acquisition, Investigation, Supervision, Validation, Writing - review & editing. **Jagpreet Singh:** Funding acquisition, Investigation, Supervision, Validation, Writing - review & editing. **Mohit Rawat:** Funding acquisition, Investigation, Supervision, Validation, Writing - review & editing.

Declaration of Competing Interest

The authors declare that they have no known competing financial interests or personal relationships that could have appeared to influence the work reported in this paper.

Acknowledgments

This research acknowledges the support made by a grant from the National Research Foundation of Korea (NRF) funded by the Ministry of Science, ICT, & Future Planning (Grant No: 2016R1E1A1A01940995).

Appendix A. Supplementary material

Supplementary data to this article can be found online at <https://doi.org/10.1016/j.envint.2020.105924>.

References

- Ahmed, M.A., Messih, M.F.A., El-Sherbeny, E.F., El-Hafez, S.F., Khalifa, A.M.M., 2017. Synthesis of metallic silver nanoparticles decorated mesoporous SnO₂ for removal of methylene blue dye by coupling adsorption and photocatalytic processes. *J. Photochem. Photobiol. A Chem.* <https://doi.org/10.1016/j.jphotochem.2017.05.048>.
- Al-Sharqi, A., Apun, K., Vincent, M., Kanakaraju, D., Bilung, L.M., 2019. Enhancement of the antibacterial efficiency of silver nanoparticles against gram-positive and gram-negative bacteria using blue laser light. *Int. J. Photoenergy*. doi:10.1155/2019/2528490.
- Ali, H., Khan, E., Ilahi, I., 2019. Environmental chemistry and ecotoxicology of hazardous heavy metals: Environmental persistence, toxicity, and bioaccumulation. *J. Chem.* <https://doi.org/10.1155/2019/6730305>.
- An, X., Long, Y., Ni, Y., 2016. Silver nanoparticle composite as a catalyst for reduction of Carbohydr. Polym. doi:10.1016/j.carbpol.2016.08.099.
- Bagherzade, G., Tavakoli, M.M., Namaei, M.H., 2017. Green synthesis of silver nanoparticles using aqueous extract of saffron (*Crocus sativus* L.) wastages and its antibacterial activity against six bacteria. *Asian Pac. J. Trop. Biomed.* <https://doi.org/10.1016/j.apjtb.2016.12.014>.
- Bansal, P., Sud, D., 2012. Photodegradation of commercial dye, CI Reactive Blue 160 using ZnO nanopowder: degradation pathway and identification of intermediates by GC/MS. *Sep. Purif. Technol.* <https://doi.org/10.1016/j.seppur.2011.09.055>.
- Baruah, D., Goswami, M., Yadav, R.N.S., Yadav, A., Das, A.M., 2018. Biogenic synthesis of gold nanoparticles and their application in photocatalytic degradation of toxic dyes. *J. Photochem. Photobiol. B Biol.* <https://doi.org/10.1016/j.jphotochem.2018.07.002>.
- Begum, R., Farooqi, Z.H., Ahmed, E., Naseem, K., Ashraf, S., Sharif, A., Rehan, R., 2016. Catalytic reduction of 4-nitrophenol using silver nanoparticles - engineered poly (N-isopropylacrylamide-co-acrylamide) hybrid microgels 1–8. doi:10.1002/aoc.3563.
- Behravan, M., Hossein Panahi, A., Naghizadeh, A., Ziaee, M., Mahdavi, R., Mirzapour, A., 2019. Facile green synthesis of silver nanoparticles using *Berberis vulgaris* leaf and root aqueous extract and its antibacterial activity. *Int. J. Biol. Macromol.* doi:10.1016/j.jbiomac.2018.11.101.
- Bingwa, N., Meijboom, R., 2014. Kinetic evaluation of dendrimer-encapsulated palladium nanoparticles in the 4-nitrophenol reduction reaction. *J. Phys. Chem. C* <https://doi.org/10.1021/jp505571p>.
- Chen, R., Yang, L., Guo, Y., Zheng, W., Liu, H., Wei, Y., 2018. Effect of p-nitrophenol degradation in aqueous dispersions of different crystallized goethites. *J. Photochem. Photobiol. A Chem.* <https://doi.org/10.1016/j.jphotochem.2017.11.028>.
- Chen, X., Zheng, Z., Ke, X., Jaatinen, E., Xie, T., Wang, D., Guo, C., Zhao, J., Zhu, H., 2010. Supported silver nanoparticles as photocatalysts under ultraviolet and visible light irradiation. *Green Chem.* <https://doi.org/10.1039/b921696k>.
- Dakshayani, S.S., Marulasiddeshwara, M.B., Sharath, S.K., Golla, R., P., R.K., Devaraja, S., Hosamani, R., 2019. Antimicrobial, anticoagulant and antiplatelet activities of green synthesized silver nanoparticles using *Selaginella* (Sanjeevini) plant extract. *Int. J. Biol. Macromol.* doi:10.1016/j.jbiomac.2019.01.222.
- Deb, S., 2014. Synthesis and characterisation of silver nanoparticles using brassica oleracea capitata (Cabbage) and phaseolus vulgaris (French Beans): A study on their antimicrobial activity and dye degrading ability. *Int. J. ChemTech Res.*
- Deng, Y., Zhao, R., 2015. Advanced Oxidation Processes (AOPs) in Wastewater Treatment. *Curr. Pollut. Reports*. doi:10.1007/s40726-015-0015-z.
- Fageria, P., Gangopadhyay, S., Pande, S., 2014. Synthesis of ZnO/Au and ZnO/Ag nanoparticles and their photocatalytic application using UV and visible light. *RSC Adv.* <https://doi.org/10.1039/c4ra03158j>.
- Fatimah, I.S., Herianto, R., 2018. Physicochemical Characteristics and Photocatalytic Activity of Silver Nanoparticles-decorated on Natural Halloysite (An aluminosilicate clay) 0–5.
- Gao, S., Zhang, Z., Liu, K., Dong, B., 2016. Applied Catalysis B: Environmental Direct evidence of plasmonic enhancement on catalytic reduction of 4-nitrophenol over silver nanoparticles supported on flexible fibrous networks. *Appl. Catal. B, Environ.* 188, 245–252. <https://doi.org/10.1016/j.apcatb.2016.01.074>.
- Gautam, A., Kshirsagar, A., Biswas, R., Banerjee, S., Khanna, P.K., 2016. Photodegradation of organic dyes based on anatase and rutile TiO₂ nanoparticles. *RSC Adv.* <https://doi.org/10.1039/c5ra20861k>.
- Gunasekar, V., Divya, B., Brinda, K., Vijaykrishnan, J., Ponnusami, V., Rajan, K.S., 2013. Enzyme mediated synthesis of Ag-TiO₂ photocatalyst for visible light degradation of reactive dye from aqueous solution. *J. Sol-Gel Sci. Technol.* <https://doi.org/10.1007/s10971-013-3134-2>.
- Huang, J., Li, Q., Sun, D., Lu, Y., Su, Y., Yang, X., Wang, H., Wang, Y., Shao, W., He, N., Hong, J., Chen, C., 2007. Biosynthesis of silver and gold nanoparticles by novel sundried Cinnamomum camphora leaf. *Nanotechnology* 18. <https://doi.org/10.1088/0957-4484/18/10/105104>.
- Jagadele, T., Kulkarni, M., Pravarthana, D., Ramadan, W., Thakur, P., 2012. Photocatalytic degradation of azo dyes using Au:TiO₂ 2, γ-Fe₃O₄:TiO₂ 2 functional nanosystems. *J. Nanosci. Nanotechnol.* <https://doi.org/10.1166/jnn.2012.5171>.
- Jain, S., Mehata, M.S., 2017. Medicinal Plant Leaf Extract and Pure Flavonoid Mediated Green Synthesis of Silver Nanoparticles and their Enhanced Antibacterial Property. *Sci. Rep.* doi:10.1038/s41598-017-15724-8.
- Jyoti, K., Baunthiyal, M., Singh, A., 2016. Characterization of silver nanoparticles synthesized using *Urtica dioica* Linn. leaves and their synergistic effects with antibiotics. *J. Radiat. Res. Appl. Sci.* 9, 217–227. <https://doi.org/10.1016/j.jrras.2015.10.002>.
- Jyoti, K., Singh, A., 2016. Green synthesis of nanostructured silver particles and their catalytic application in dye degradation. *J. Genet. Eng. Biotechnol.* 14, 311–317. <https://doi.org/10.1016/j.jgeb.2016.09.005>.
- Kale, M.J., Avanesian, T., Christopher, P., 2014. Direct photocatalysis by plasmonic nanostructures. *ACS Catal.* <https://doi.org/10.1021/cs400993w>.
- Kalishwaralal, K., BarathManiKanth, S., Pandian, S.R.K., Deepak, V., Gurunathan, S., 2010. Silver nanoparticles impede the biofilm formation by *Pseudomonas aeruginosa* and *Staphylococcus epidermidis*. *Colloids Surfaces B Biointerfaces*. <https://doi.org/10.1016/j.colsurfb.2010.04.014>.
- Kästner, C., Thünemann, A.F., 2016. Catalytic reduction of 4-nitrophenol using silver nanoparticles with adjustable activity. *Langmuir* 32, 7383–7391. <https://doi.org/10.1021/acs.langmuir.6b01477>.
- Khan, Mujeeb, Khan, Merajuddin, Adil, S.F., Tahir, M.N., Tremel, W., Alkhatlan, H.Z., Al-Warhan, A., Siddiqui, M.R.H., 2013. Green synthesis of silver nanoparticles mediated by *Pulicaria glutinosa* extract. *Int. J. Nanomedicine*. doi:10.2147/IJN.S43309.
- Khandelwal, R., Arora, S.K., Phase, D.M., Pareek, A., 2020. Anti cancer potential of green synthesized silver nanoparticles. *Anti Cancer Potential of Green Synthesized Silver* 020046.
- Khanna, A., Shetty, V.K., 2014. Solar light induced photocatalytic degradation of Reactive Blue 220 (RB-220) dye with highly efficient Ag@TiO₂ core-shell nanoparticles: A comparison with UV photocatalysis. *Sol. Energy*. doi:10.1016/j.solener.2013.10.032.
- Khanna, D.P., More, P.V., 2018. Electro-photocatalytic degradation of methylene blue dye using various nanoparticles: A demonstration for undergraduates 7, 254–257. <https://doi.org/10.15406/jnmr.2018.07.00195>.
- Khataee, A.R., Kasiri, M.B., 2010. Photocatalytic degradation of organic dyes in the presence of nanostructured titanium dioxide: Influence of the chemical structure of dyes. *J. Mol. Catal. A Chem.* <https://doi.org/10.1016/j.molcata.2010.05.023>.
- Kodom, T., Rusen, E., Colinescu, I., Mocanu, A., Somoghi, R., Dinescu, A., Diacon, A., Boscornea, C., 2015. Silver nanoparticles influence on photocatalytic activity of hybrid materials based on TiO₂ P25. *J. Nanomater.* <https://doi.org/10.1155/2015/210734>.
- Kumar, P., Govindaraju, M., Senthamselvi, S., Premkumar, K., 2013. Photocatalytic degradation of methyl orange dye using silver (Ag) nanoparticles synthesized from *Ulva lactuca*. *Colloids Surfaces B Biointerfaces*. <https://doi.org/10.1016/j.colsurfb.2012.11.022>.
- Lee, B., Lee, M.J., Yun, S.J., Kim, K., Choi, I.H., Park, S., 2019. Silver nanoparticles induce reactive oxygen species-mediated cell cycle delay and synergistic cytotoxicity with 3-bromopyruvate in *Candida albicans*, but not in *Saccharomyces cerevisiae*. *Int. J. Nanomedicine*. doi:10.2147/IJN.S205736.
- Leong, K.H., Aziz, A.A., Sim, L.C., Saravanan, P., Jang, M., Bahemann, D., 2018. Mechanistic insights into plasmonic photocatalysts in utilizing visible light. *Beilstein J. Nanotechnol.* doi:10.3762/bjnano.9.59.
- Li, S., Shen, Y., Xie, A., Yu, X., Qiu, L., Zhang, L., Zhang, Q., 2007. Green synthesis of silver nanoparticles using *Capsicum annuum* L. extract. *Green Chem.* 9, 852. <https://doi.org/10.1039/b615357g>.
- Lu, A.S., Yu, J., Cheng, Y., Barras, A., Xu, W., Szunerits, S., Cornu, D., Boukherroub, R., 2017. Preparation of silver nanoparticles / polydopamine functionalized polyacrylonitrile fiber paper and its catalytic activity for the reduction 4-nitrophenol. *Appl. Surf. Sci.* doi:10.1016/j.apsusc.2017.03.120.
- Mariselvam, R., Ranjitsingh, A.J.A., Mosae Selvakumar, P., Alarfaj, A.A., Munusamy, M. A., 2016. Spectral studies of UV and solar photocatalytic degradation of AZO dye and textile dye effluents using green synthesized silver nanoparticles. *Bioinorg. Chem. Appl.* doi:10.1155/2016/8629178.
- Mavaei, M., Chahardoli, A., Shokoohinia, Y., Khoshroo, A., Fattahi, A., 2020. One-step Synthesized Silver Nanoparticles Using Isoimperatorin: Evaluation of Photocatalytic, and Electrochemical Activities. *Sci. Rep.* doi:10.1038/s41598-020-58697-x.
- Mody, V., Siwale, R., Singh, A., Mody, H., 2010. Introduction to metallic nanoparticles. *J. Pharm. Bioallied Sci.* 2, 282. <https://doi.org/10.4103/0975-7406.72127>.

- Mohan, S., Devan, M.V., 2019. Photocatalytic activity of Ag/Ni bi-metallic nanoparticles on textile dye removal. *Green Process. Synth.* doi:10.1515/gps-2019-0060.
- Muhd Julkapli, N., Bagheri, S., Bee Abd Hamid, S., 2014. Recent advances in heterogeneous photocatalytic decolorization of synthetic dyes. *Sci. World J.* doi:10.1155/2014/692307.
- Nawaz, M.S., Ahsan, M., 2014. Comparison of physico-chemical, advanced oxidation and biological techniques for the textile wastewater treatment. *Alexandria Eng. J.* <https://doi.org/10.1016/j.aej.2014.06.007>.
- Niu, Z., Li, Y., 2014. Removal and utilization of capping agents in nanocatalysis. *Chem. Mater.* doi:10.1021/cm4022479.
- O'Connor, O.A., Young, L.Y., 1989. Toxicity and anaerobic biodegradability of substituted phenols under methanogenic conditions. *Environ. Toxicol. Chem.* doi:10.1002/etc.5620081003.
- Online, V.A., Lee, K., 2015. RSC Advances. doi:10.1039/C5RA11892A.
- Paul, N.S., Sharma, R., Yadav, R.P., 2015. Biological synthesis of antimicrobial silver nanoparticles by *Phaseolus vulgaris* seed extract. *MGM J. Med. Sci.* 2, 1–6. <https://doi.org/10.5005/jp-journals-10036-1036>.
- Peiris, M.M.K., Fernando, S.S.N., Jayaweera, P.M., Arachchi, N.D.H., Guansekara, T.D.C.P., 2018. Comparison of antimicrobial properties of silver nanoparticles synthesized from selected bacteria. *Indian J. Microbiol.* 58, 301–311. <https://doi.org/10.1007/s12088-018-0723-3>.
- Petita, A., Florea, A., Gaidau, C., Balan, D., Anicai, L., 2019. Synthesis and characterization of silver-titanium nanocomposites prepared by electrochemical method with enhanced photocatalytic characteristics, antifungal and antimicrobial activity. *J. Mater. Res. Technol.* <https://doi.org/10.1016/j.jmrt.2017.09.009>.
- Pirtarighat, S., Ghannadnia, M., Baghshahi, S., 2019. Green synthesis of silver nanoparticles using the plant extract of *Salvia spinosa* grown in vitro and their antibacterial activity assessment. *J. Nanostructure Chem.* 9, 1–9. <https://doi.org/10.1007/s40097-018-0291-4>.
- Raj Pant, H., Pant, B., Joo Kim, H., Amarjargal, A., Hee Park, C., Tijing, L.D., Kyo Kim, E., Sang Kim, C., 2013. A green and facile one-pot synthesis of Ag-ZnO/RGO nanocomposite with effective photocatalytic activity for removal of organic pollutants. *Ceram. Int.* doi:10.1016/j.ceramint.2012.12.003.
- Raveendran, P., Fu, J., Wallen, S.L., 2003. Completely “Green” Synthesis and Stabilization of Metal Nanoparticles. *J. Am. Chem. Soc.* doi:10.1021/ja029267j.
- Ravichandran, V., Vasanthi, S., Shalini, S., Adnan, S., Shah, A., Tripathy, M., Paliwal, N., 2019. Results in physics photocatalytic activity of *Parkia speciosa* leaves extract mediated silver nanoparticles. *Results Phys.* 15, 102565. <https://doi.org/10.1016/j.rinp.2019.102565>.
- Reverberi, A.P., Kuznetsov, N.T., Meshalkin, V.P., Salerno, M., Fabiano, B., 2016. Systematical analysis of chemical methods in metal nanoparticles synthesis. *Theor. Found. Chem. Eng.* doi:10.1134/S0040579516010127.
- Rolim, W.R., Pelegrino, M.T., de Araújo Lima, B., Ferraz, L.S., Costa, F.N., Bernardes, J.S., Rodrigues, T., Brocchi, M., Seabra, A.B., 2019. Green tea extract mediated biogenic synthesis of silver nanoparticles: Characterization, cytotoxicity evaluation and antibacterial activity. *Appl. Surf. Sci.* doi:10.1016/j.apsusc.2018.08.203.
- Roy, A., Bulut, O., Some, S., Mandal, A.K., Yilmaz, M.D., 2019. Green synthesis of silver nanoparticles: Biomolecule-nanoparticle organizations targeting antimicrobial activity. *RSC Adv.* <https://doi.org/10.1039/c8ra08982e>.
- Roy, K., Sarkar, C.K., Ghosh, C.K., 2015a. Photocatalytic activity of biogenic silver nanoparticles synthesized using yeast (*Saccharomyces cerevisiae*) extract. *Appl. Nanosci.* doi:10.1007/s13204-014-0392-4.
- Roy, K., Sarkar, C.K., Ghosh, C.K., 2015b. Photocatalytic activity of biogenic silver nanoparticles synthesized using potato (*Solanum tuberosum*) infusion. *Spectrochim. Acta - Part A Mol. Biomol. Spectrosc.* doi:10.1016/j.saa.2015.02.058.
- Roy, K., Sarkar, C.K., Ghosh, C.K., 2015c. Photocatalytic activity of biogenic silver nanoparticles synthesized using potato (*Solanum tuberosum*) infusion. *Spectrochim. Acta - Part A Mol. Biomol. Spectrosc.* doi:10.1016/j.saa.2015.02.058.
- Saeed, M., Muneer, M., Khosa, M.K.K., Akram, N., Khalid, S., Adeel, M., Nisar, A., Sherazi, S., 2019. *Azadirachta indica* leaves extract assisted green synthesis of Ag-TiO₂ for degradation of Methylene blue and Rhodamine B dyes in aqueous medium. *Green Process. Synth.* doi:10.1515/gps-2019-0036.
- Shaik, M.R., Khan, Mujeeb, Kuniyil, M., Al-Warthan, A., Alkhatlan, H.Z., Siddiqui, M.R.H., Shaik, J.P., Ahmed, A., Mahmood, A., Khan, Merajuddin, Adil, S.F., 2018. Plant-Extract-Assisted green synthesis of silver nanoparticles using *Origanum vulgare* L. Extract and their microbicidal activities. *Sustain.* doi:10.3390/su10040913.
- Shaikh, W.A., Chakraborty, S., Islam, R.U., 2019. Photocatalytic degradation of rhodamine B under UV irradiation using *Shorea robusta* leaf extract-mediated bio-synthesized silver nanoparticles. *Int. J. Environ. Sci. Technol.* doi:10.1007/s13762-019-02473-6.
- Singh, J., Dutta, T., Kim, K.-H., Rawat, M., Samddar, P., Kumar, P., 2018a. ‘Green’ synthesis of metals and their oxide nanoparticles: applications for environmental remediation. *J. Nanobiotechnology* 16, 84. <https://doi.org/10.1186/s12951-018-0408-4>.
- Singh, J., Kaur, N., Rawat, M., 2018b. Eco-friendly approach for synthesis of AgNPs and their catalytic application toward 4-nitrophenol to 4-aminophenol reduction. *Micro Nano Lett.* 13, 1600–1603. <https://doi.org/10.1049/mnl.2018.5139>.
- Singh, J., Kukkar, P., Sammi, H., Rawat, M., Singh, G., Kukkar, D., 2017. Enhanced catalytic reduction of 4-nitrophenol and congo red dye by silver nanoparticles prepared from *Azadirachta indica* leaf extract under direct sunlight exposure. *Part. Sci. Technol.* 1–10. <https://doi.org/10.1080/02726351.2017.1390512>.
- Singh, J., Kumar, V., Singh Jolly, S., Kim, K.-H., Rawat, M., Kukkar, D., Tsang, Y.F., 2019. Biogenic synthesis of silver nanoparticles and its photocatalytic degradation for removal of organic pollutants in water. *J. Ind. Eng. Chem.* 1–11. <https://doi.org/10.1016/j.jiec.2019.08.002>.
- Singh, K., Arora, S., 2011. Removal of synthetic textile dyes from wastewaters: A critical review on present treatment technologies. *Crit. Rev. Environ. Sci. Technol.* doi:10.1080/10643380903218376.
- Sinha, T., Ahmaruzzaman, M., 2015. High-value utilization of egg shell to synthesize Silver and Gold-Silver core shell nanoparticles and their application for the degradation of hazardous dyes from aqueous phase-A green approach. *J. Colloid Interface Sci.* 453, 115–131. <https://doi.org/10.1016/j.jcis.2015.04.053>.
- Slavin, Y.N., Asnis, J., Häfeli, U.O., Bach, H., 2017. Metal nanoparticles: Understanding the mechanisms behind antibacterial activity. *J. Nanobiotechnology.* <https://doi.org/10.1186/s12951-017-0308-z>.
- Sreekanth, T.V.M., Jung, M.J., Eom, I.Y., 2016. Green synthesis of silver nanoparticles, decorated on graphene oxide nanosheets and their catalytic activity. *Appl. Surf. Sci.* doi:10.1016/j.apsusc.2015.11.146.
- Subash, B., Krishnakumar, B., Swaminathan, M., Shanthi, M., 2013. Highly efficient, solar active, and reusable photocatalyst: Zn-loaded Ag-ZnO for reactive red 120 dye degradation with synergistic effect and dye-sensitized mechanism. *Langmuir.* <https://doi.org/10.1021/ja303842c>.
- Suchomel, P., Kvitek, L., Prucek, R., Panacek, A., Halder, A., Vajda, S., Zboril, R., 2018. Simple size-controlled synthesis of Au nanoparticles and their size-dependent catalytic activity. *Sci. Rep.* doi:10.1038/s41598-018-22976-5.
- Suliman, M.A., Gondal, M.A., Dastageer, M.A., Chuah, G.K., Basheer, C., 2019. Method for visible light-induced photocatalytic degradation of methylparaben in water using nanostructured Ag/AgBr@m-WO₃. *Photochem. Photobiol.* 95, 1485–1494. <https://doi.org/10.1111/php.13118>.
- Sumi, M.B., Devadiga, A., Shetty, K.V., Saidutta, M.B., 2017. Solar photocatalytically active, engineered silver nanoparticle synthesis using aqueous extract of mesocarp of *Cocos nucifera* (Red Spicata Dwarf). *J. Exp. Nanosci.* <https://doi.org/10.1080/17458080.2016.1251622>.
- Telke, A., Kalyani, D., Jadhav, J., Govindwar, S., 2008. Kinetics and mechanism of reactive red 141 degradation by a bacterial isolate *Rhizobium radiobacter* MTCC 8161. *Acta Chim. Slov.*
- Thawarkar, S.R., Thombare, B., Munde, B.S., Khupse, N.D., 2018. Kinetic investigation for the catalytic reduction of nitrophenol using ionic liquid stabilized gold nanoparticles. *RSC Adv.* <https://doi.org/10.1039/c8ra07404f>.
- Trapido, M., Kallas, J., 2000. Advanced oxidation processes for the degradation and detoxification of 4-nitrophenol. *Environ. Technol. (United Kingdom)* 21, 799–808. <https://doi.org/10.1080/09593330.2000.9618966>.
- Udani, J., Tan, O., Molina, J., 2018. Systematic review and meta-analysis of a proprietary alpha-amylase inhibitor from white bean (*Phaseolus vulgaris* L.) on weight and fat loss in humans. *Foods.* doi:10.3390/foods7040063.
- Van Dong, P., Ha, C.H., Binh, L.T., Kasbohm, J., 2012. Chemical synthesis and antibacterial activity of novel-shaped silver nanoparticles. *Int. Nano Lett.* doi:10.1186/2228-5326-2-9.
- Vanaamudan, A., Soni, H., Padmaja Sudhakar, P., 2016. Palm shell extract capped silver nanoparticles - As efficient catalysts for degradation of dyes and as SERS substrates. *J. Mol. Liq.* <https://doi.org/10.1016/j.molliq.2016.01.027>.
- Verma, A.D., Jain, N., Singha, S.K., Quraishi, M.A., Sinha, I., 2016. Green synthesis and catalytic application of curcumin stabilized silver nanoparticles 128, 1871–1878. <https://doi.org/10.1007/s12039-016-1189-7>.
- Vieira, G.B., José, H.J., Peterson, M., Baldissarelli, V.Z., Alvarez, P., de Fátima Peralta Muniz Moreira, R., 2018. CeO₂/TiO₂ nanostructures enhance adsorption and photocatalytic degradation of organic compounds in aqueous suspension. *J. Photochem. Photobiol. A Chem.* doi:10.1016/j.jphotochem.2017.11.045.
- Wang, L., Hu, C., Shao, L., 2017. The antimicrobial activity of nanoparticles: Present situation and prospects for the future. *Int. J. Nanomedicine.* doi:10.2147/IJN.S121956.
- Wang, L., Lu, F., Liu, Y., Wu, Y., Wu, Z., 2018. Photocatalytic degradation of organic dyes and antimicrobial activity of silver nanoparticles fast synthesized by flavonoids fraction of *Psidium guajava* L. leaves. *J. Mol. Liq.* 263, 187–192. <https://doi.org/10.1016/j.molliq.2018.04.151>.
- Wani, I.A., Ganguly, A., Ahmed, J., Ahmad, T., 2011. Silver nanoparticles: Ultrasonic wave assisted synthesis, optical characterization and surface area studies. *Mater. Lett.* doi:10.1016/j.matlet.2010.11.003.
- Xiao, S., Xu, W., Ma, H., Fang, X., 2012. Size-tunable Ag nanoparticles immobilized in electrospun nanofibers: Synthesis, characterization, and application for catalytic reduction of 4-nitrophenol. *RSC Adv.* 2, 319–327. <https://doi.org/10.1039/c1ra00127b>.
- Yadi, M., Mostafavi, E., Saleh, B., Davaran, S., Aliyeva, I., Khalilov, R., Nikzamid, M., Nikzamid, N., Akbarzadeh, A., Panahi, Y., Milani, M., 2018. Current developments in green synthesis of metallic nanoparticles using plant extracts: a review. *Artif. Cells, Nanomedicine Biotechnol.* doi:10.1080/21691401.2018.1492931.
- Yola, M.L., Eren, T., Atar, N., Wang, S., 2013. Adsorptive and photocatalytic removal of reactive dyes by silver nanoparticle-colemanite ore waste. *Chem. Eng. J.* doi:10.1016/j.cej.2013.12.086.
- Zhang, X.F., Liu, Z.G., Shen, W., Gurnathan, S., 2016. Silver nanoparticles: Synthesis, characterization, properties, applications, and therapeutic approaches. *Int. J. Mol. Sci.* doi:10.3390/ijms17091534.
- Zhang, Y., Fu, F., Li, Y., Zhang, D., Chen, Y., 2018. One-step synthesis of Ag@TiO₂ nanoparticles for enhanced photocatalytic performance. *Nanomaterials* 8. <https://doi.org/10.3390/NANO8121032>.
- Zhao, P., Feng, X., Huang, D., Yang, G., Astruc, D., 2015. Basic concepts and recent advances in nitrophenol reduction by gold- and other transition metal nanoparticles. *Coord. Chem. Rev.* doi:10.1016/j.ccr.2015.01.002.